Geomorphology 118 (2010) 152–166

Contents lists available at ScienceDirect

Geomorphology

journal homepage: www.elsevier.com/locate/geomorph

Rockfall susceptibility map for Athinios port, Santorini Island, Greece

Andreas A. Antoniou [a,*], Efthimios Lekkas [b]

[a] National Technical University of Athens, Department of Geotechnical Engineering, Athens, Greece
[b] Department of Dynamic Tectonic Applied Geology, Faculty of Geology and Geoenvironment, National and Kapodistrian University of Athens, Greece

ARTICLE INFO

Article history:
Received 18 February 2009
Received in revised form 15 December 2009
Accepted 19 December 2009
Available online 29 December 2009

Keywords:
Rockfall
Santorini
Geomorphology
Reach angle
Susceptibility map
GIS

ABSTRACT

This article analyzes rockfall susceptibility in the steep caldera slopes upstream of Athinios port, Santorini Island, Greece. The study area is situated in the internal rim of a submarine caldera where the most important problem that is recorded is the frequent rockfalls that not only cause damages to roads and vehicles but also pose a threat to people that are transported or located on the port. As a result, a methodology which combines information relatively to surficial and engineering geology, geomorphological processes, and structural analysis was adopted. The methodology incorporates evenly a maximum runout map generated by means of reach probability of rock block analysis, using the empirical model of "reach angle". Additionally volumes of rockfall events categorized and presented through a map to assist the compilation of rockfall susceptibility map which allows us to identify areas and human activities exposed to these incidents and set up several protection meters.

1. Introduction

Rockfall is an impendent phenomenon present in many slopes throughout the world (Hoek, 2007; Chen et al., 2009). Rockfalls range from small cobbles to large boulders hundreds of cubic meters in size, and travel at speeds ranging from few to tens of meters per second. Although the relatively small size of a rock block these falls are a major cause of landslide fatalities particularly along roads and characterized by high energy and mobility. Their dynamic processes are dominated by spatially and temporally distributed attributes, such as detachment conditions, geometry features and mechanical properties (static and dynamic friction, roughness, rolling resistance, restitution characteristics and fragmentation ratio) of both rock blocks and slopes (Agliardi and Crosta, 2003).

Human activities on a rock slope are exposed to this incident; so the revelation of zones free of rockfall is of major significance. Minor rockfalls affect most of the rock slopes, whereas large rockfalls affect only great rock slopes with geological conditions favorable to instability (Rouiller et al., 1998). At mountainous areas where the rockfall hazard increases, the slope and rock properties controlling the initiation and behaviour of rockfalls vary widely. Studies of rockfalls are usually based on field surveys, and the hazard is estimated either by susceptibility to failure or by the calculation of a safety factor derived from rock mechanics models (Hoek and Bray, 1981; Ayala-Cardeco et al., 2003).

Coe and Harp (2007) indicate that rockfall travel distance on rock slopes is analyzed from empirical models. Several differences between rockfalls and other types of landslides for susceptibility analysis can be found: (i) runout is very different (generally related to block size); (ii) trace of block movement, especially the older ones, are generally absent; and (iii) at commonly used scales, the blocks from rockfall cannot be cartographically displayed (Ayala-Cardeco et al., 2003).

This article introduces a methodology to evaluate the susceptibility of minor rockfall of a road located on steep caldera slopes upstream Athinios port, in the internal rim of a submarine caldera on the Santorini Island complex (Fig. 1), and is based on geological, geomorphological parameters, structural analysis, rockfall maximum runout of rock blocks by adopting the empirical model of "reach angle" and rockfall events. The accuracy of the empirical model verified with experimental rockfall carried out on the slope. The compilation of the abovementioned parameters led to rockfall susceptibility map through GIS environment and allows us to construct several protection meters.

2. Methodology for GIS-aided rockfall susceptibility map

2.1. General

Since the mid 1980s, geographical information system (GIS) becomes a very popular technology used in calculating and managing natural hazards, including landslides. GIS analysis has also been proposed to produce rockfall hazard map (e.g. Cancelli and Crosta,

* Corresponding author. National Technical University of Athens, Department of Geotechnical Engineering, 9 Iroon Polytechniou St, 157 80, Zografou, Athens, Greece. Tel.: +30 21 07723421; fax: +30 21 07723428.
E-mail address: andreasan19@yahoo.com (A.A. Antoniou).

0169-555X/$ – see front matter © 2009 Elsevier B.V. All rights reserved.
doi:10.1016/j.geomorph.2009.12.015

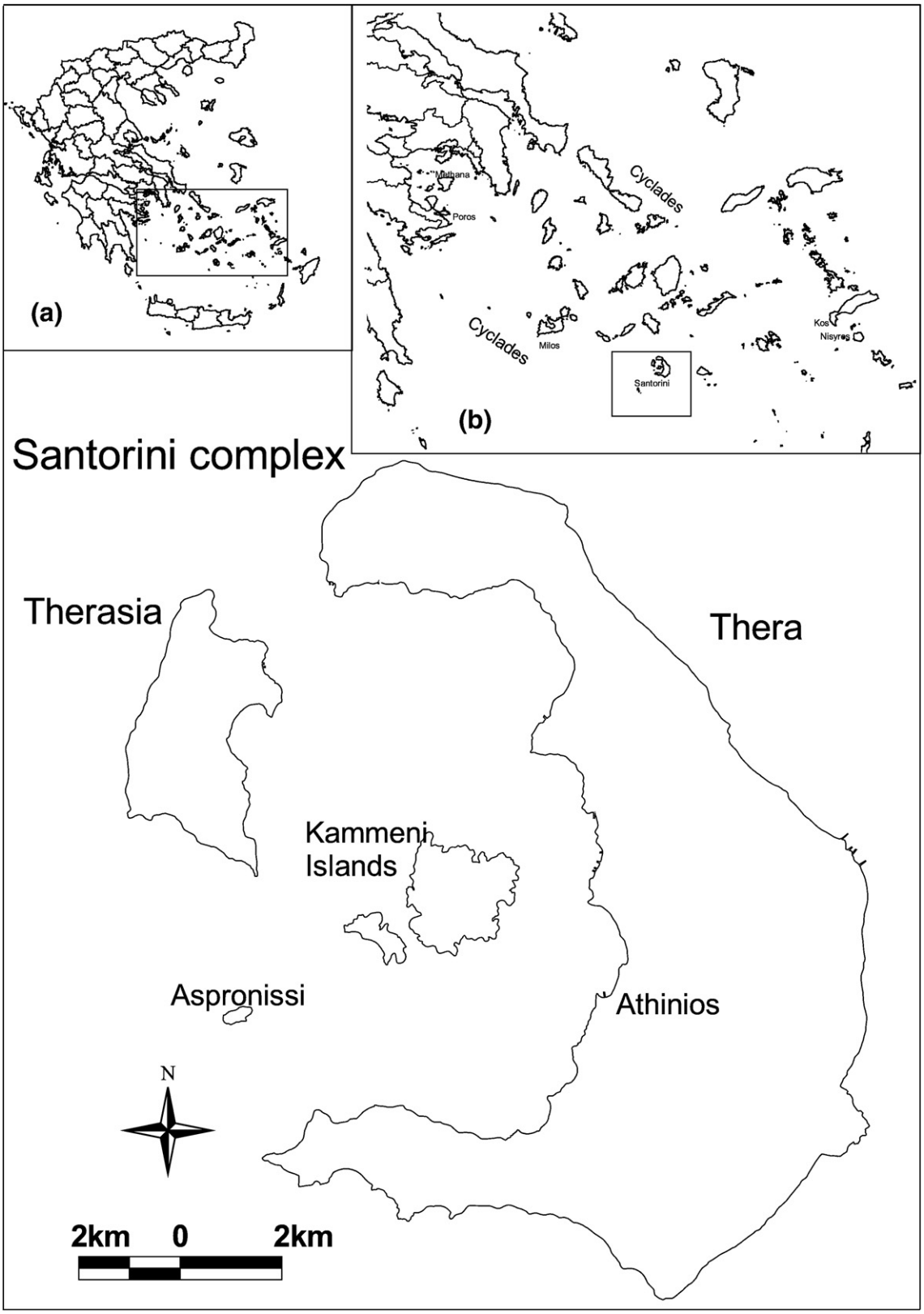

Fig. 1. Map of Santorini Island.

1994). Baillifard et al. (2003) presented a methodology for rockfall hazard mapping using GIS-based parameters such as topography, geomorphology and geology. They refer that these parameters derived from the location of the observed rockfall and they can be easily mapped and integrated in a GIS. Dorren and Seijmonsbergen (2003) developed GIS-based distributed model which calculates the rockfall velocity on the basis of energy loss due to collisions with trees and on the soil surface. Chau et al. (2004) presented a framework of

generating rockfall hazard map based on rockfall inventory and GIS, where the slope angle, slope aspect and elevation at each of these rockfall locations are generated using GIS-based digital elevation model (DEM). Lan et al. (2007) presented a GIS extension, RockFall Analyst (RA), which is capable of effectively handling large amounts of geospatial information relative to rockfall behaviors.

2.2. Outline of methodology

Fig. 2 presents a simplified flow chart of the proposed methodology that uses as input:

- Geological information on the basis of structural analysis for the selected area,
- Geomorphological information such as slope angle and slope aspect,
- Rockfall runouts, and
- Rockfall files.

According to their regime, geological formations present discontinuities, joints and faults, very often unfavorable to natural or manmade slopes. A detailed structural analysis demonstrates their dip/dip direction and indicates the potential type of failure. When dip joints reveal rock blocks on top of slope, prone to rockfall, then the formation rates to categories from 1 to 5 (increased tendency to rockfall).

In general, steeper slopes exhibit more frequently rockfalls, as a consequence of gravity effects. A digital elevation model classifies slope to slope units, from 1 to 9 (0° to 90° dip).

Numerical or analytical rockfall runout modeling requires the determination of the geometrical and physical characteristics of the falling block and of the slope. The principal geometrical features refer to the block size and the shape, while the principal physical characteristics are the initial free falling block velocity, the coefficient of restitution and the energy loss at impact. The principal slope instability modes are sliding and toppling, but in case of sufficiently rounded unstable block shape, rolling movement may be induced. Rockfall runouts categorized according to their impact on human activities, 1 (low impact) to 3 (significant impact).

For the study area, a rockfall file based on in situ observations, aerial photo interpretation, or historical documents constitutes the basis of rockfall susceptibility analysis. The rockfall trajectories back analyze with RockFall program in order to show the agreement between the rockfall parameters value adopted for the study area and the substantial trajectory. The rockfall initial point also demonstrates the crescive tendency for rockfall from this geological formation.

The summation of the foregoing parameters led to the compilation of the rockfall susceptibility map through GIS environment.

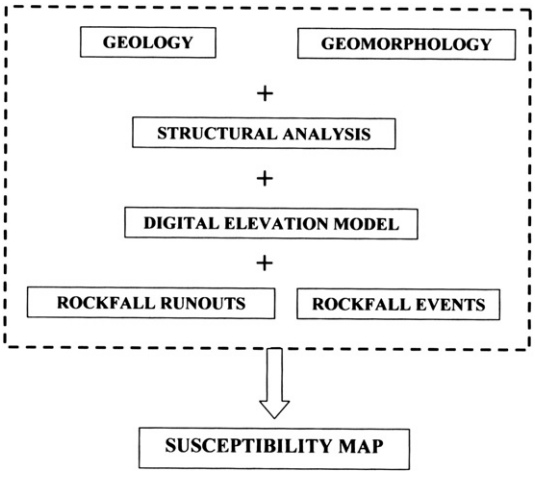

Fig. 2. Flow chart of the proposed methodology.

3. Geology of the study area

Coe and Harp (2007) indicate that rockfall susceptibility on rock slopes, at a detailed scale, is analyzed on the basis of a thorough geological survey. The detailed geological survey revealed the appearance of the following units extended in the study area.

Upper pumice (geological unit A): concerns rhyodacitic, white to whitish, coarse grained at its base to fine grained at its top pumice. Frequently, bodies of lava or scoriae up to 2 m are present. At the base of the formation massive yellowish pumice is noted with a maximum thickness of 10 m. According to Druitt and Francaviglia (1992), the age of the formation is 3.6 ka (Minoan eruption), while the maximum visible thickness at the study area is about 50 m (Fig. 3a).

Upper scoriae (geological unit B): reddish scoriae and pyroclastic materials alternations with maximum thickness of 20 m to the north of the study area while they disappear to the south. According to Druitt and Francaviglia (1992), the age of the formation is 54 ± 3 ka and belongs to the second pumice eruption (Fig. 3b).

Intermediate tuffs (geological unit C): concerns an alternated sequence of pumices, scoriaes, ignimbrites, breccias and lavas. The thickness is about 40 m and belongs to the second pumice eruption while superjacent to the prevolcanic formations in the central part of the study area (Fig. 3c).

Lower pumice (geological unit D): this unit is divided into two horizons: the upper consists of reddish to yellowish pumice (geological unit D1) and includes lava's bodies while its thickness varies from 20 to 30 m. The lower horizon consists of reddish pumices, ignimbrites, scoriaes, and breccias (geological unit D2) and has a total thickness of about 30 m, while two layers of whitish pumice can be distinguished at its subordinate part. According to Druitt and Francaviglia (1992), the age of the formation is 203 ± 23 ka and belongs to first pumice eruption (Fig. 3d).

Andesitic pyroclast (geological unit D3): comprise a sequence of black to reddish andesitic scoriae, robustly cemented, breccia and tuffs that are superjacent to the pre-volcanic formations (Fig. 3e). The width of this unit, upward of Athinios port is 30 m.

Phyllites (geological unit E): this unit belongs to the prevolcanic island of late Mesozoic to Tertiary (Tataris, 1964) and mainly consists of marbles, schists, and calcareous phyllites. The formation is heavily jointed and brecciated because of the volcanic eruption (Fig. 3f).

Debris (geological unit F): formation comprising from fragments of phyllites or lava, which is the remnant of the Minoan landslip described by Druitt and Francaviglia (1992) (Fig. 3g). Its thickness is usually <5 m and because of heavy rainfalls the formation is prone to downstream movements.

Manmade activities (unit G): Concerns the road to the port, the facilities of the port, as well as the buildings around the port.

The abovementioned geological units presented through the ArcView GIS environment (ESRI, 1996), in a geological map (Fig. 4).

4. Geomorphology of island and study area

The Cyclades region is a metamorphic complex area that formed in Triassic to Tertiary time and was folded and metamorphosed during Alpine folding around 60 million years ago. The Island complex of Santorini comprises the Islands of Thera, Therasia, Nea Kammeni, Palaia Kammeni (Kammeni Islands) and Aspronissi. While its shape is nearly circular, the largest island, Thera, has a semi-circular shape concaves toward the west, while Therasia and Aspronissi are located in the western section of the complex and all together form a ring around the gigantic submarine caldera. Thera is located in the central

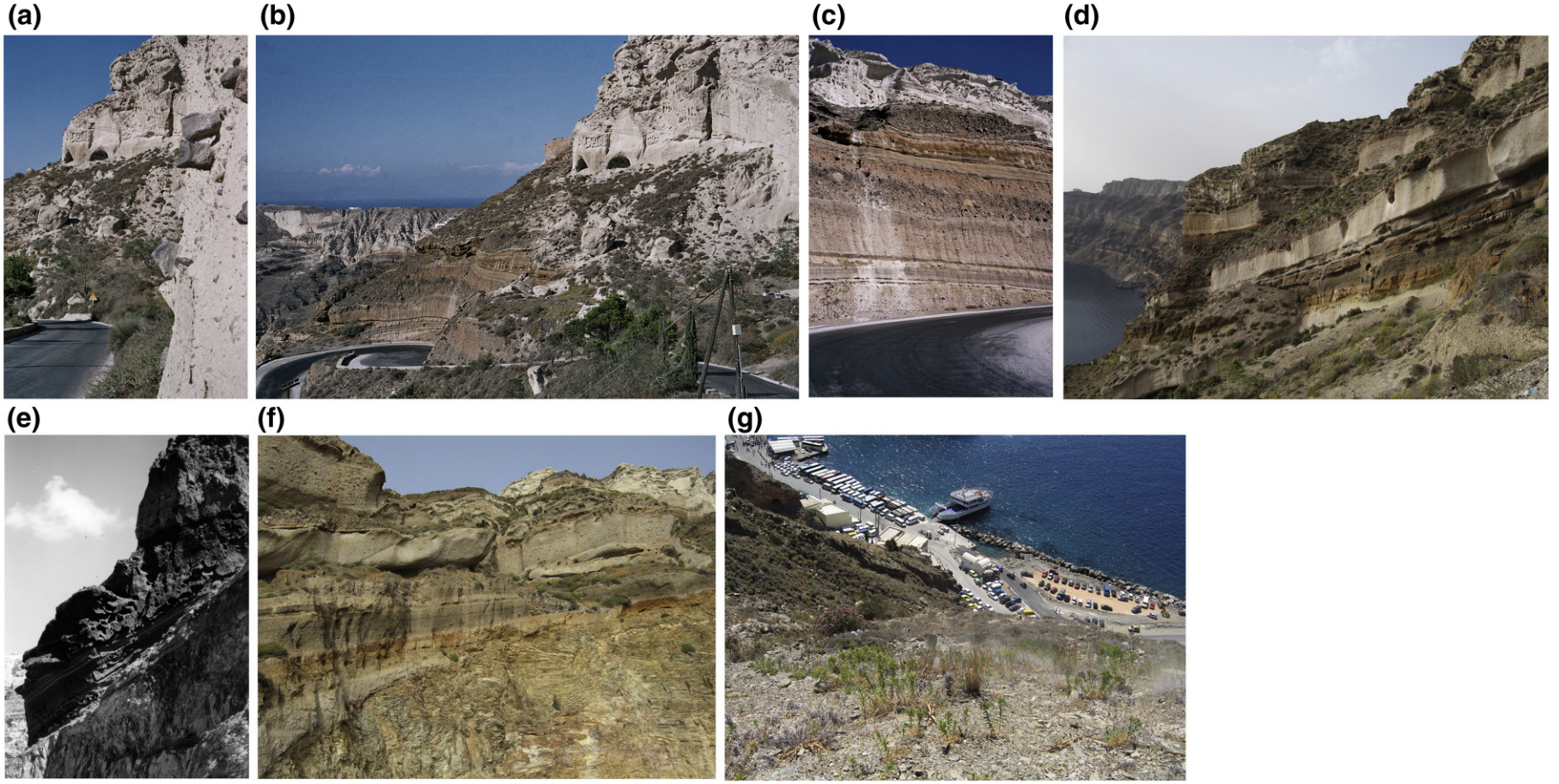

Fig. 3. a. Upper pumice (geological unit A). b. Upper scoriae (geological unit B). c. Intermediate tuff (geological unit C). d. Yellowish pumice (geological unit D1) and reddish pumice (geological unit D2). e. Andesitic pyroclast (geological unit D3). f. Prevolcanic formations (geological unit E). g. Scree (geological unit F).

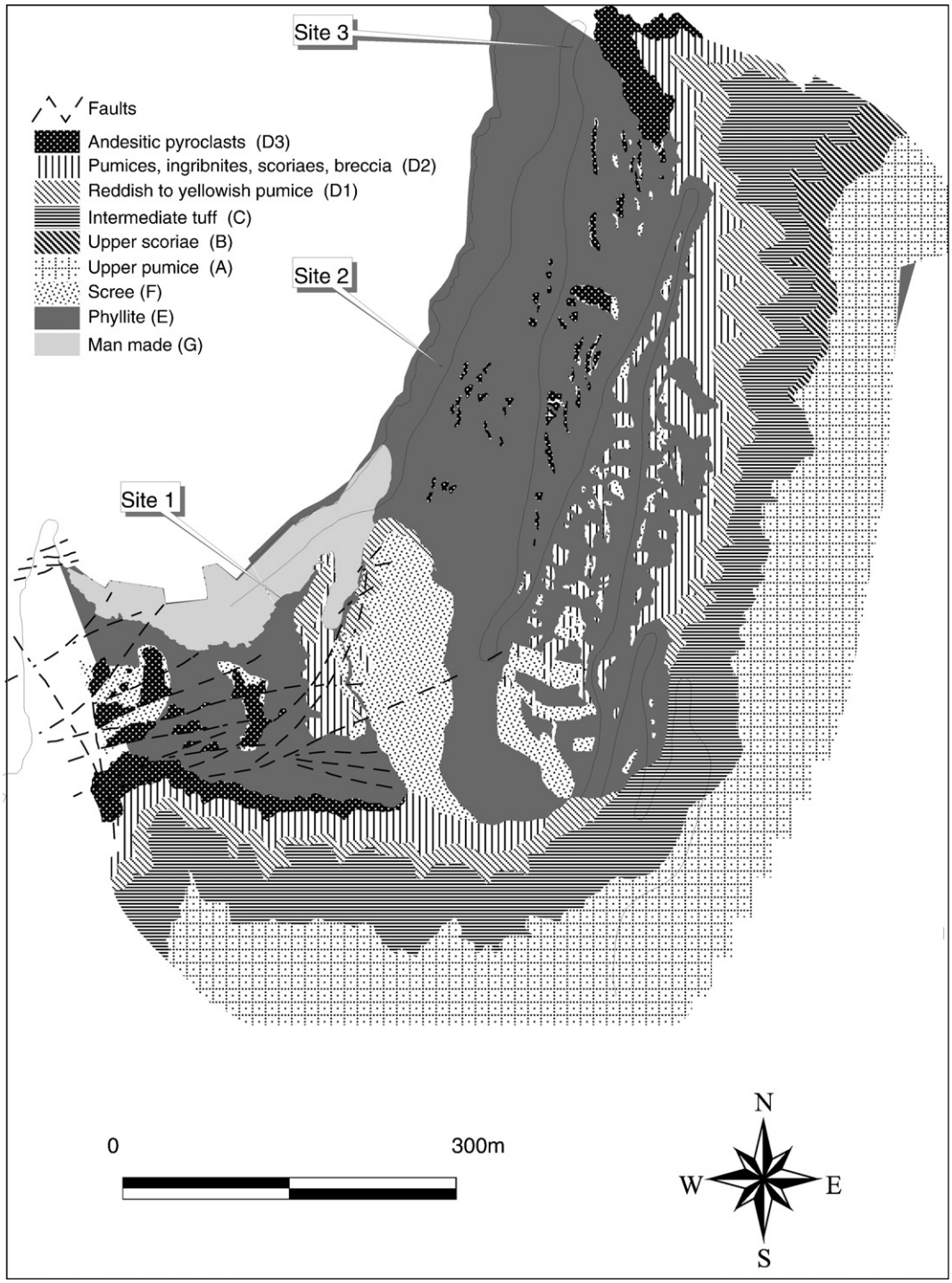

Fig. 4. Geological map of the study area.

part of the Hellenic volcanic arc, which also includes the volcanic centres of Sousaki, Methana, Poros, Milos, Kos and Nisyros. This arc has a length of 500 km and width ~20 to 40 km, extending from the Saronikos gulf through the southern Aegean and reaches the west coast of Turkey. The volcanic activity initiated 3 million years ago and is attributed to the subduction of the African plate under the Eurasian plate. Around 1640 B.C. vast explosion known as the Minoan eruption took place in the region of Santorini, while the explosions of 197 B.C. and 726 A.D. formed Palaia Kammeni and through the eruptions of 1570, 1707, 1886, 1925, 1940–41, and 1950 Nea Kammeni formed (Washington, 1926; Ktenas, 1926a,b; Georgalas and Liatsikas, 1932; Georgalas, 1953; Georgalas and Papastamtiou, 1953). Those two islets are located in the center of the aforementioned ring and these eruptions were followed by intense, intermediate depth earthquakes related to magma upwelling from the melting of the sinking slab. The volcanic activity in Santorini is represented by the presence of many small volcanic centers that produced a great variety of volcanic formations constructing a typical stratovolcano with a conic shape and sequential deposits. The caldera diameter in the N–S direction is ~ 11 km and in the E–W direction it is around 7 km. The maximum depth of the caldera below mean sea level is approaching 380 m. The height of the caldera walls above sea level is ~300 m. The highest

Fig. 5. View of the southern slope of Athinios port.

elevation, 564 m, of the island complex is recorded in Thera at the mountain of Profitis Ilias, located to the SE of the island.

According to Druitt and Francaviglia (1992), the caldera wall exposes an ancient cliff of the prevolcanic island. This unconformity is draped and plastered by pyroclastics, adhering patches that extend to less than 100 m above sea level. They propose that the Minoan collapse exhumed this unconformity, leaving a veneer of onlapping pyroclastics. Uncovering cannot predate the Minoan eruption because the Minoan pumice does not plaster the unconformity like the fall deposits of older eruptions. Druitt and Francaviglia (1992), also report that the southern part of the caldera wall has scalloped shapes that are attributed to rotational landslip during or soon after the Minoan collapse. Lipman (1976) indicated that such slips are common occurrences during caldera formation and can result in significant enlargement of the caldera beyond the main collapse faults. The landslip deposits that form the prominent coastal cusp at Athinios consist of blocks of intact or brecciated schist overlain by slumped and partly remobilized pyroclastics, while the northern edge of the landslip is covered by talus breccias containing Minoan pumice (Druitt and Francaviglia, 1992).

The study area is located upward of Athinios port and divided in two sections: the northern part unfolds from north to south, with

Fig. 6. View of the eastern slope of Athinios port and the road that leads to the port.

slope angle equal to 32° to west, while the southern part extends from NW to SE and dips 37° to north. Despite the fact that the southern part exhibits many morphological discontinuities which generate a scalloped shape, its maximum elevation does not exceed 250 m (Fig. 5), while the uppermost part of northern slope presents a prevailing discontinuity and the elevation is over 300 m (Fig. 6).

The major fault zone directed from east to south determined geological boundaries between prevolcanic and volcanic formations while lower pumice (geological unit D) suffered almost 20 m vertical movement. Upper pumice (geological unit A) remained intact from the fault action although Alpine formations (geological unit E) heavily jointed and brecciated.

4.1. Slope angle

Slope failures occur more readily on steeper slopes due to gravity stresses (Cook and Doornkamp, 1990). Since steeper slopes present a higher potential for failure, the materials that make up such slopes

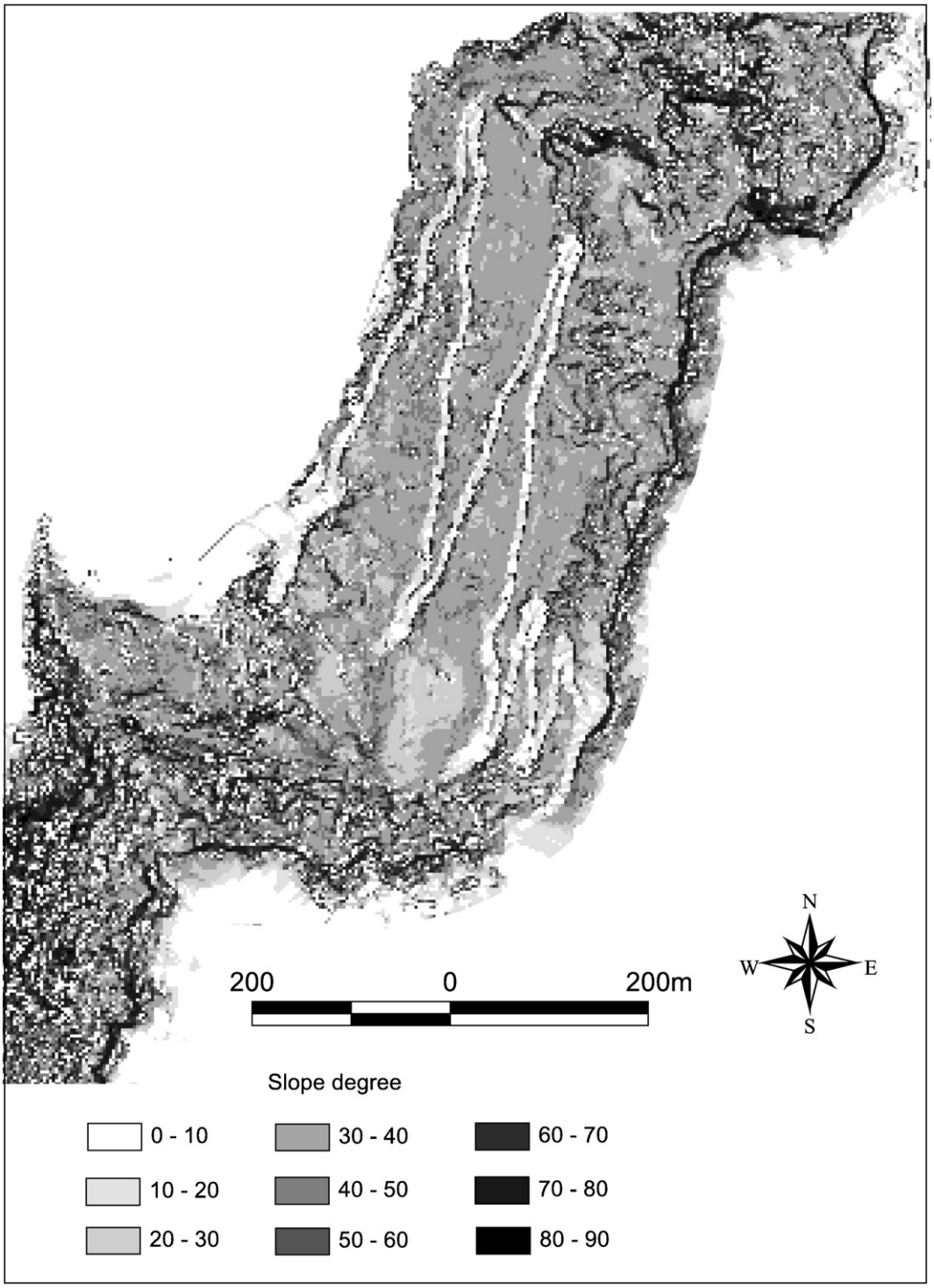

Fig. 7. Slope map of the study area.

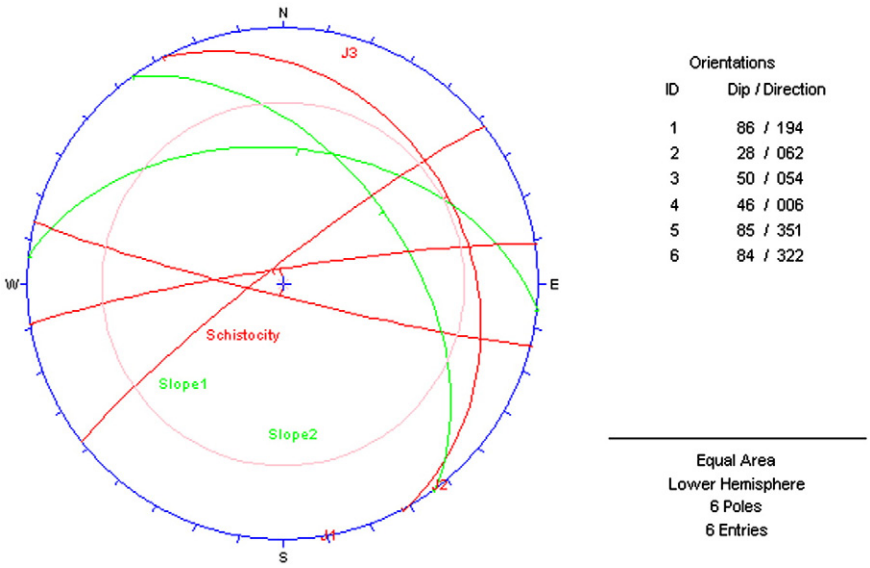

Fig. 8. Major joints orientation sets and slopes for site 1.

with steep angles can be expected to be stronger. (Chen et al., 2009). Therefore, the trade-off between the increasing driving force and increasing material strength as slopes with steep angles may mitigate the impact of slope angle (Roth 1983).

For the study area, slope angle is <45° and only the higher part of the slope where upper pumice extends, the slope angle is >60° (Fig. 7), while the slope height is >20 m. Moreover, the angle of manmade slopes excavated for the road is >60°, but their height is usually <5 m.

5. Structural analysis

According to geological formations extending to the study area, the occurrence of typical rock slope failure such as planar, wedge, and toppling exhibit only heavily jointed and brecciated from major fault activity geological unit E. In consequence, a detailed geological survey for this unit was carried out on the basis of 150 different in situ measurements on joint orientations gathered from three sites (the port area and two sites along road; see Fig. 4).

The International Society for Rock Mechanics (ISRM) suggests a series of methods or the quantitative description of discontinuities in rock masses (ISRM, 1978). Among the identification parameters for such discontinuities, the mechanical behavior of a rock mass is greatly determined by its joints; therefore, the joint set number of a rock slope is an influence parameter on stability (ISRM, 1978). The major joint orientation sets as well as slope orientations, at study area, are presented in Figs. 8 (site 1), 9 (site 2) and 10 (site 3). Joints were closed and tights, except to the excavated faces along the road where a small aperture (<1 mm) was observed. The friction angle along joint surface was considered, in a conservative approach, 30° allowing wedge failures to occur. Joints orientation defines the volume of rockfall block, resulting in volumes of 0.5 to 1.5 m^3 in phyllites (equivalent weight of 1,1 to 3,6 tn) to be observed. Table 1 presents the proportion of unstable rock blocks, along with their volume classification.

The other geological units such as pumices, tuffs, and pyroclasts are well bonded to phyllites or among each other and cannot exhibit planar or wedge failure. The steep slopes of upper pumice constitute

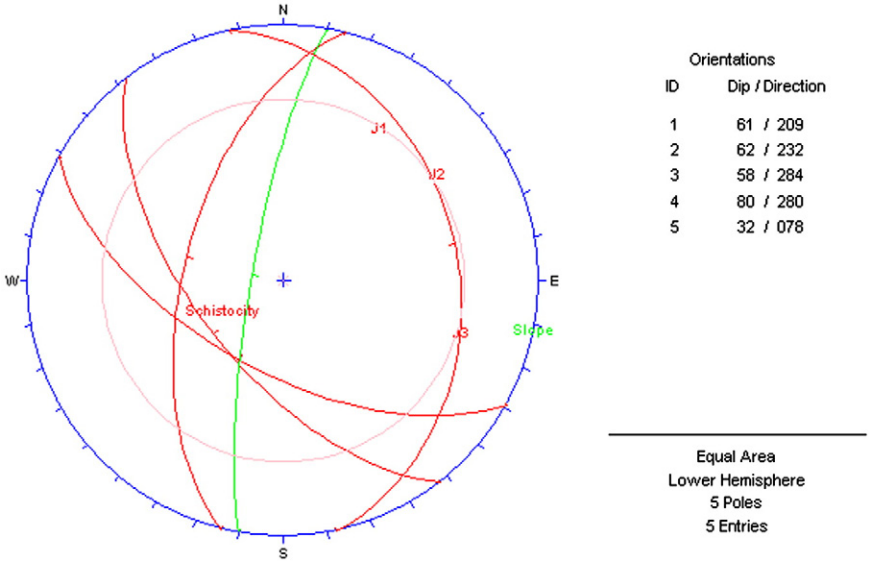

Fig. 9. Major joints orientation sets and slopes for site 2.

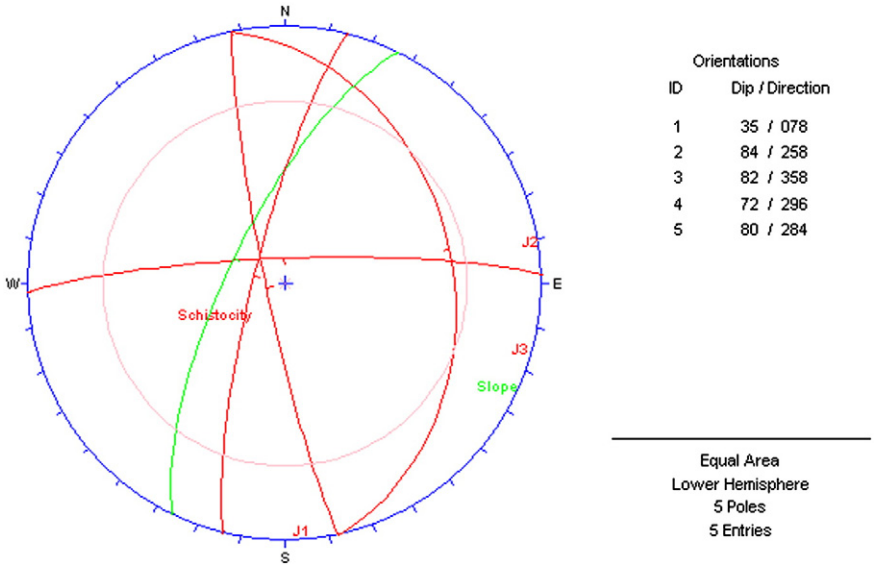

Fig. 10. Major joints orientation sets and slopes for site 3.

remarkable exception, because the activity of weathering and gravity produced many tension cracks. The maximum detached but not yet fallen rock block volumes estimated to 25 m^3, resulting to 51tn rock boulder.

6. Rockfall runout

6.1. General

A rockfall is usually controlled by slope roughness, volume of blocks, and energy loss at impact; while the maximum runout distance is directly associated to the previous factors as well as the initial velocity of a rockfall.

The rock block detached by sliding, toppling or falling, which falls along a vertical or sub-vertical cliff, proceeds down slope by bouncing and flying along ballistic trajectories or by rolling on talus or debris slopes (Varnes, 1978). When the block has lost enough energy in impacts or by friction it stops on or at the foot of the slope. After release, a rock-fall trajectory is thus the combination of four main processes, namely: sliding and/or toppling, free falling, bouncing (impact) and rolling (Broili, 1973). These processes are controlled by well-known physical (mechanical) laws and can be described by simple equations (Guzzetti et al., 2002).

Azzoni et al. (1995) found that the main characteristics of a rockfall model are the assessment of velocities, height of bounces, and energies achieved during the fall as well as the assessment of maximum runout distances in order to determine the areas at risk. They also report that given the substantial variability of the rockfall phenomenon, it has been necessary to define all those variables within a range centered on their mean value, and to make a numerical simulation using the Monte Carlo method, by choosing within the mentioned range, the values of all the variables at random.

Table 1
Proportion and volume of unstable rock blocks.

Geotechnical unit	Proportion		
	<0.5 m^3	0.5–1.5 m^3	>1.5 m^3
A	2%	36%	62%
E	68%	26%	6%

Guzzetti et al. (2002) present the software code “STONE” which makes use of a DTM and some thematic maps derived by geo-lithologic, land use, geomorphologic and landslide inventory maps.

6.2. Slope roughness

The texture of geological units extended to the study area as well as the impact of weathering to them produces a slope surface that is rather uneven. Consequently, slope roughness has been estimated in situ and presents low values, < 5°, in upper pumice (geological unit A), upper scoriae (geological unit B), lower pumice (geological unit D1), lower scoriae (geological unit D2), and debris (geological unit F); moderate values in intermediate tuff, between 5° and 8° (geological unit C); while the values are significantly higher in andesitic pyroclast (geological unit D3) and in phyllites (geological unit E), between 8°and 12°.

6.3. Volume of blocks

Based on in situ observations detached rock blocks volumes equal to 25 m^3 were present in upper pumice (geological unit A). The following scenario was adopted in the analyses presented hereinafter (for rock blocks detached from geological unit A): 51 tn rock boulder starts a free fall, and after the first impact, this boulder separates in to three pieces of 17 tn each that continue the fall (Fig. 11). The initial velocity of this rock boulder is calculated by equalizing the dynamic energy obtained from free fall with the kinetic energy just before impact. This is a very conservative approach since upper pumice (geological unit A) presents elastic behavior and usually absorbs a significant amount of energy during impact. When geological unit E outcrops the detailed structural analysis specified the volume of rock blocks (in general their volume varied from 0.5 m^3 to 1.5 m^3).

6.4. Energy loss at impact

Giani (1992) report that during the flight, the block has a constant energy ‘head’ equal to:

$$E = z + \frac{V^2}{2g} \quad (1)$$

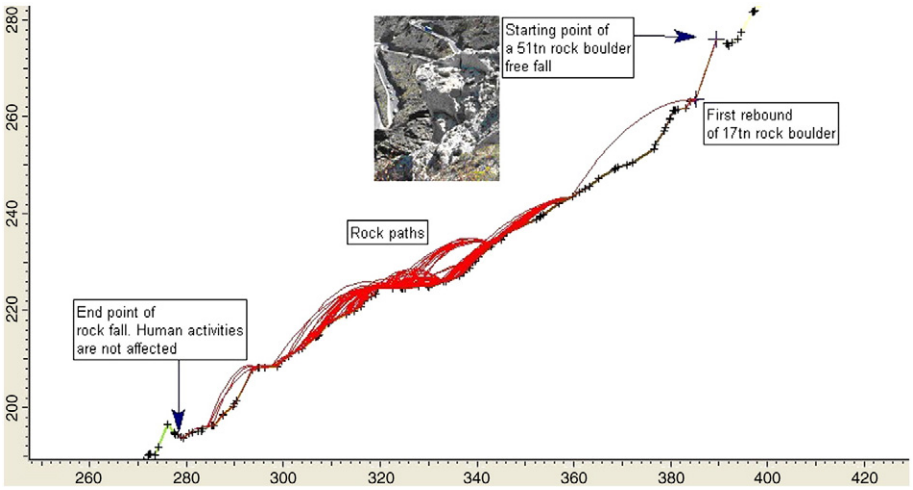

Fig. 11. Rock path for a detached rock block from geological unit A.

where z is the block elevation and V is the block velocity. After the impact, the resulting incremental loss of energy is determined as:

$$E = \frac{V^2}{2g}\left(\frac{K_t^2 + K_n^2 \tan^2\beta'}{1 + \tan^2\beta'} - 1\right) \quad (2)$$

where β' is the angle of incidence prior to the impact.

According to the Newton theory of particle collision (in Giani, 1992) the coefficient K is defined as:

$$K = \frac{v_2' - v_1'}{v_2 - v_1} \quad (3)$$

where v_i represents the initial particle velocity and v_i' the final velocity after the collision of two particles 1 and 2. In the case of a block falling to the ground, the coefficient K can be simplified as:

$$K = \frac{v'}{v} \quad (4)$$

where v and v' are the block velocities before and after the impact respectively.

For free falling, Eq. (4) becomes:

$$K = \sqrt{\frac{h'}{h}} \quad (5)$$

where h and h' represent the original falling height and the rebound height after the impact respectively.

Imre et al. (2008) refer that the energy loss of a rock boulder at impact is controlled by the coefficient of restitution. The most commonly used definitions for the coefficient of restitution are the tangential (R_t) and normal (R_n) components where

$$R_n = \frac{V_{rn}}{V_{in}} \quad (6)$$

$$R_t = \frac{V_{rt}}{V_{it}} \quad (7)$$

where V_{rn} and V_{rt} are the magnitudes of the normal and tangential component of the rebounding velocities, whilst V_{in} and V_{it} refer to the magnitude of the same components of the incoming velocities (Chau et al., 2002). Those coefficients of restitution depend on the angle of impact, the impact energy level, and the deformability of rock boulders and rock slopes. While many scale tests have been executed at sedimentary and metamorphic rocks for the estimation of coefficient of restitution, few data referring to volcanic formations have been published. Budetta and Santo (1994) using back analyses methods carried out in Atrani, Campagnia, Southern Italy obtained values of 0.10 and 0.20 for the R_n and R_t coefficients, respectively, concerning the remolded pyroclastic deposits from the terraces situated at the base of the cliff. They concluded that those values were sufficiently reliable, especially if they compared to those obtained experimentally by Urciuoli (1988, in Budetta and Santo, 1994) who studied the impacts on detritus of the fans presented at the foot of rock cliffs at the old Italcementi quarries and obtained a practically zero value for R_n and 0.24 for R_t.

For the purposes of the analyses, the values for R_n and R_t in volcanic formations were specified from experiments carried out on the slope. In particular two scale tests were executed in order to reevaluate kinematical parameters of the blocks: the experiments consisted of handmade recorded falls with an initial velocity of a 50 kg[3] rock bolder; in addition, an estimation of the unconfined compression test was based on the in situ Schmidt hammer type L test. The test was executed on the upper pumice formation, as well as pyroclastic formation and middle tuff. The test, contraindicates to pyroclastic material because of its structure, nevertheless was carried out as a denotation. The mean values for the three formations ($N = 14$, $N = 15$ and $N = 14$) pointed out that those volcanic material are characterized as soft rocks that could absorb the kinetic energy of the rock boulder. The results of the runout tests used to adjust the kinematical parameters of rock blocks, and finally the R_n and R_t values for the geological units extended to the entire slope are presented to Table 2.

Table 2
Values for geotechnical parameters R_n, R_t and friction angle.

Description	Geotechnical unit	Friction angle φ	R_n		R_t	
			Mean value	Standard deviation	Mean value	Standard deviation
Upper pumice	A	26	0.25	0.04	0.70	0.04
Upper scoriae	B	28	0.35	0.04	0.80	0.04
Lower pumice, medium tuff	C, D1, D2, D3	24	0.20	0.04	0.70	0.04
Phyllites	E	30	0.35	0.04	0.85	0.04
Scree	F	30	0.30	0.04	0.80	0.04
Asphalt	G	30	0.40	0.04	0.90	0.04

6.5. Initial velocity of a rockfall

The initial block velocity, at the beginning of the fall, depends on the initial instability mode and on the block displacement that occurs before the block is thrown into the air (Giani, 1992). The rock slope instability mode may be induced by water pressure in joints, earthquake shaking (Kobayashi et al., 1990; Lin et al., 2006a,b) or blast vibrations, slope excavation, etc. The principal slope instability modes are sliding and toppling; but when the unstable block shape is sufficiently rounded, then a rolling movement may be induced. Consequently the block rolling or sliding velocity v after length l is calculated as

$$v = 2\sqrt{g(\sin\alpha - \tan\theta\cos\alpha)l} \quad (3)$$

where g is gravity acceleration, θ is the sliding or rolling friction angle, and α is the slope inclination.

The initial velocity of rock boulder in seismic conditions was calculated, taking into account the regional macroseismic activity. The island complex of Santorini presents moderate seismicity and, according to historical and recent instrumented data, the complex has suffered from many earthquakes. Table 3 summarizes the seismic events that occurred within a distance of <100 km from the broader area of Santorini Island (according to Papazachos and Papazachou, 1997). While the Greek Seismic Code EAK suggests seismic ground acceleration equal to 0.24 g for Santorini Island Complex, the above-mentioned regional macroseismic activity point out the increment of seismic ground acceleration; thus $a = 0.30$ g was adopted. Assuming that the seismic wave removes the rock fragment away from the slope equal to 5 cm (distance $s = 5$ cm) and by equalizing dynamic mass inertia to kinetic energy, the initial velocity of a rock boulder is calculated as follows

$$\frac{1}{2}m^*v^2 = m^*a^*s > v = \sqrt{2^*a^*s} \quad (4)$$

6.6. Analysis of travel distances using empirical models

Nineteen cross sections were selected for the entire study area, where several block propagation analyses were carried out using the RocFall program of Rocscience Ltd under static as well as seismic loading conditions.

Several authors have substantiated that the larger rock block generate larger runout for the same morphology. Ayala-Cardeco et al. (2003) refer that rock blocks with more cubic or spherical morphologies have a larger runout than noncubic or nonspherical ones. According to Copons and Vilaplana (2008), rockfalls with similar sizes do not always have identical travel distances. Moreover, rock blocks from a given rockfall have neither identical travel distances nor the same runout. Therefore, a rockfall susceptibility zoning on human activities requires an analysis of reach probability of rock blocks. In our case, rock blocks with higher runouts have volumes ranging from 0.5 to 1.5 m^3, the larger one having higher runout.

For the study area, the susceptibility analysis was executed by analyzing travel distances, through the selection of a reliable empirical model. Two main empirical models are used to predict travel distances: the "reach angle" model, which is the dipping of the line connecting the rockfall source to the fallen rock block (Corominas, 1996); and the "shadow angle" model, which is the dipping of the line connecting the fallen block to the top of the talus slope (Evans and Hungr, 1993). For the study area, the "reach angle" model was considered more appropriate, as no talus slope exists. According to Rouiller et al. (1998, in Copons and Vilaplana, 2008), the reach probability is the frequency of falling rock blocks that

Table 3
Seismic events that occurred within a distance of less than 100 km from the broader area of Santorini complex, according to Papazachos and Papazachou (1997).

Year	Epicenter	Magnitude/intensity	Remarks
198 B.C.	36.4° N, 25.4° E	$M_s = <6$	The epicenter located between island of Thera and Therasia. The earthquake is attached to volcanic activity
46 A.D.	36.4° N, 25.4° E	$M_s = 6.5$	The earthquake is attached to volcanic activity
1650 October 9	36.5° N, 25.5° E	$M_s = 7$/VIII	40 people killed, 200 houses collapsed, a 30 m height tsunami hit the coastal line of Crete island
1707 September. 2	36.4° N, 25.4° E	$M_s = < 6$	Volcanic activity and creation of Nea Kammeni island
1733 December 23	37.1° N, 24.8° E	$M_s = 6.5$/VIII	Damages at Sifnos and Paros islands
1735	36.8° N, 24.5° E	$M_s = 6.5$/VIII	Damages at Milos island
1810 February 16	35.5°N, 25.6°E (Heraklion, Crete)	$M_s = 7.8$/IX	
1846 March 28	35.8°N, 25.0°E (Heraklion, Crete)	$M_s = 7.7$/VIII	
1856 October 12	35.6°N, 26.0°E (Heraklion, Crete)	$M_s = 8.2$/IX	Severe damages at Crete and Santorini, many churches collapse at Santorini
1862 June 21	36.9°N, 24.4° E	$M_s = 7$/VIII	Few damages at Milos, Folegandros, Sifnos and Santorini
1866 January 31	36.4°N, 25.4° E	$M_s = 6.1$/VII	Damages at 50 houses and churches
1887 July 17	35.7°N, 26.0° E (Heraklion, Crete)	$M_s = 7.5$/VII	
1956 July 9	36.64° N, 25.96° E	$M_s = 7.5$/IX	Severe damages at Santorini, Amorgos, Anafi, Astypalaia, Ios, Paros, Naxos, Kalymnos, Leros and Patmos islands. 53 people killed, 529 houses collapsed, 1482 with severe damages. A 20 to 25 m height tsunami hit the NW coastal line of Astypalaia and SW coastal line of Amorgos

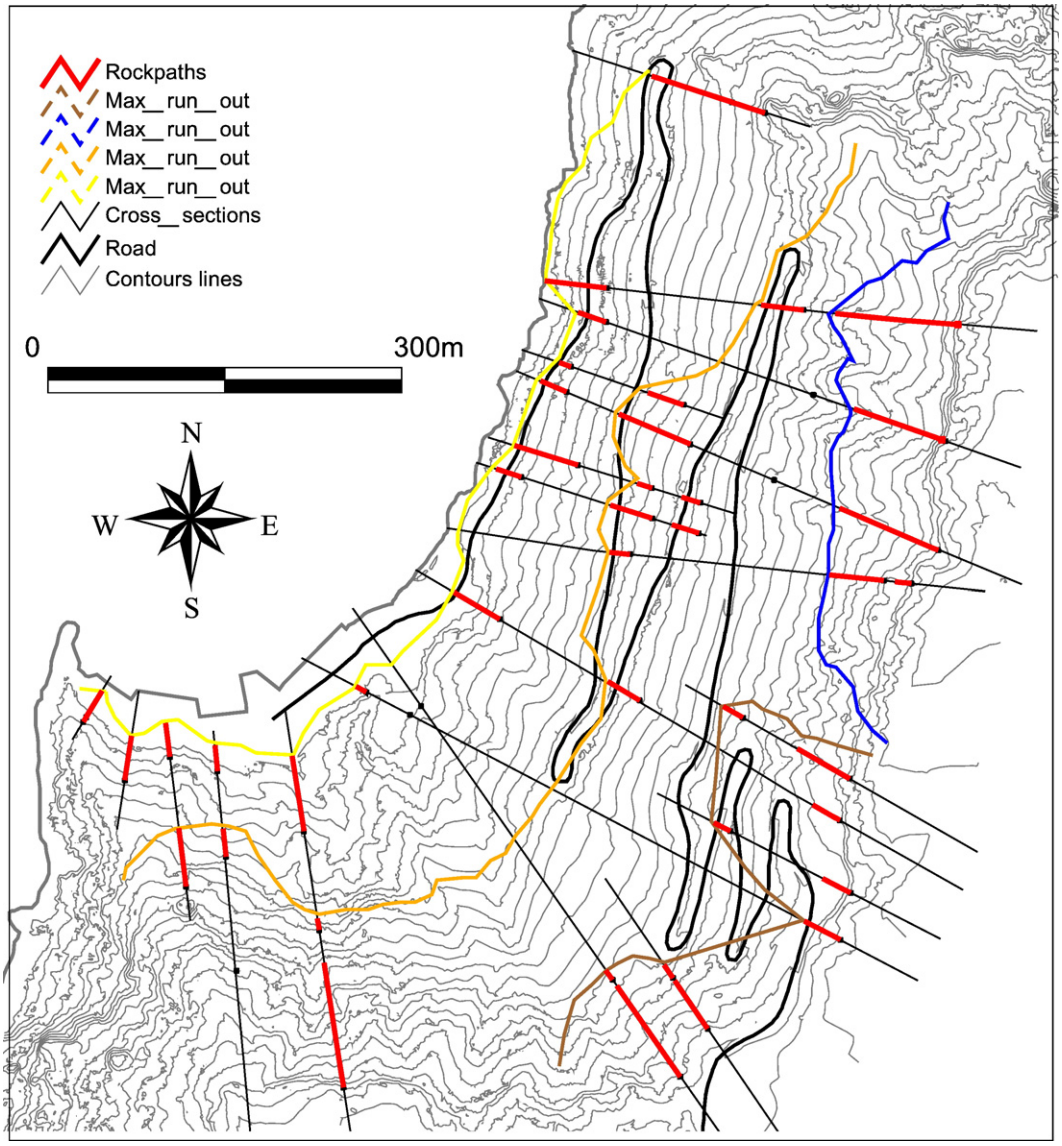

Fig. 12. Maximum runout lines for four different elevation levels.

could reach a point of the exposed area. A statistical analysis of 38 places inside the study area prone to rockfall has been used to obtain the reach angle for the "reach angle" empirical model. The results of the statistical analysis demonstrate that this reach limit can be placed using a reach angle of 35° (see Fig. 11). The "reach limit" line is obtained by joining points with the same reach limit. This line has been used to analyze travel distances within the study area. From fieldwork, the more distant rock blocks were mapped, as well as from random block propagation analyses; in all 19 sections, the maximum runouts were also recorded. Finally, a line interpolated among them was produced: the maximum runout line. Interpolation has been carried out for the entire slope at four different elevation levels, having in mind the slope homogeneity, the continuous presence of the scarp along the study area and the human activities (Fig. 12).

6.7. Rockfall files

For the study area, a rockfall file based on in situ observations, aerial photo interpretation and eyewitnesses, or historical documents constitutes the basis of rockfall susceptibility analysis. Rainfall influences the triggering of rockfall as shown by the fact that most of the events happen shortly after heavy rainfall episodes, according to historical documents and evidence from eyewitnesses. However, no direct relationship was confirmed between rainfall amount and rockfall size. The trajectories of those rockfall were simulated through RocFall program adopting rockfall parameters resulted from the foregoing analyses. Additionally the entire slope investigated with the intention to locate the beginning of rockfall, while these simulations demonstrate that the rockfall parameters were properly selected. Fig. 13 reproduces the territorial distribution of recorded rockfalls.

7. Rockfall susceptibility map for human activities

The need for safer use of the road in all elevation levels, upstream Athinios port, as well as port facilities at Santorini Island, pointed out the necessity of a 20 m buffer zone along them. As a consequence, the rockfall susceptibility map referring to human activities as they developed to different elevations is presented in Fig. 14, wherein the following zones were determined.

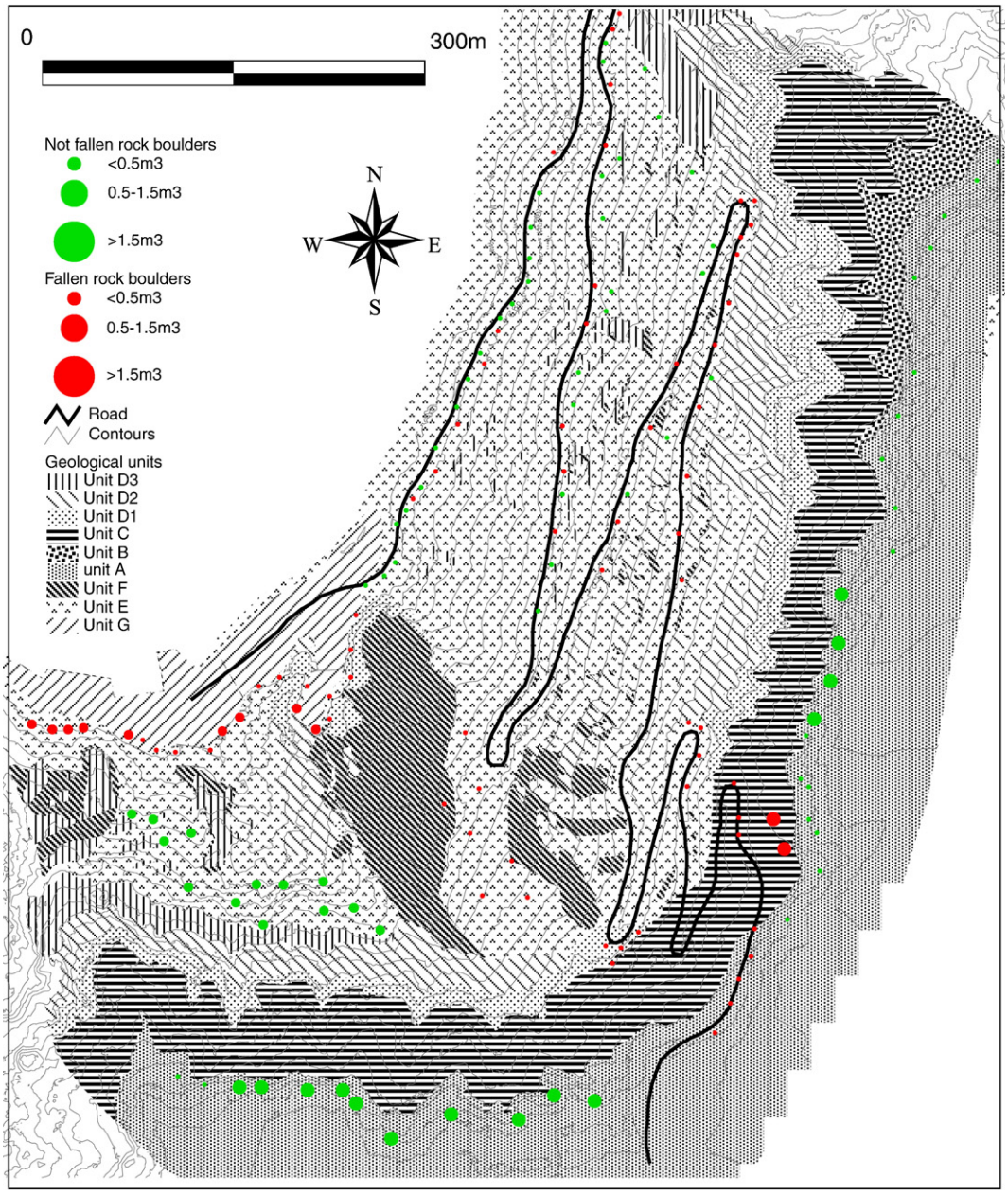

Fig. 13. Territorial distribution of recorded rockfalls.

Zone A: susceptibility in this zone is not only by reach but also by instability phenomena from slopes along the road and port facilities. There is the possibility of almost free-fall at manmade slopes along the road; hence this zone has been named as a High Susceptibility zone and treatment with protection measures is recommended. Those measures will be determined by analyzing rock paths in every section involved in the zone, especially bounce height and total kinetic energy produced during rockfall. As a consequence, rockfall barrier systems with absorbing energy equal to the developed kinetic energy will be installed along the road. The analyses results show that, typically low energy rockfall fences with one brake ring are applicable.

Zone B: It is susceptible for a rock boulder to reach, but human activities are away from this zone. Therefore has been named the Moderate Susceptibility zone. Protection measures will be applied only if justified by analysis at a more detailed scale.

Zone C: susceptibility in this zone is mainly from instability phenomena from steep slopes. The possibility of free-fall is very prominent. It has been named the Low Susceptibility zone given that human activities are far away from this zone. No protection measures are needed.

8. Conclusions

This article introduces a methodology to evaluate the susceptibility of minor rockfall of a road located on steep caldera slopes upstream Athinios port. Thematic maps were compiled to illustrate geological information, rockfall maximum runout of rock blocks and rockfall events. In addition geomorphological parameters and structural analysis were taken into account, while the geologic material related to rockfall phenomena has not been presented before. The rockfall runout evaluated by adopting the empirical model of “reach angle” while the accuracy of the empirical model verified with experimental rockfall carried out on the slope. The outcome of this process is the rockfall susceptibility map through GIS environment.

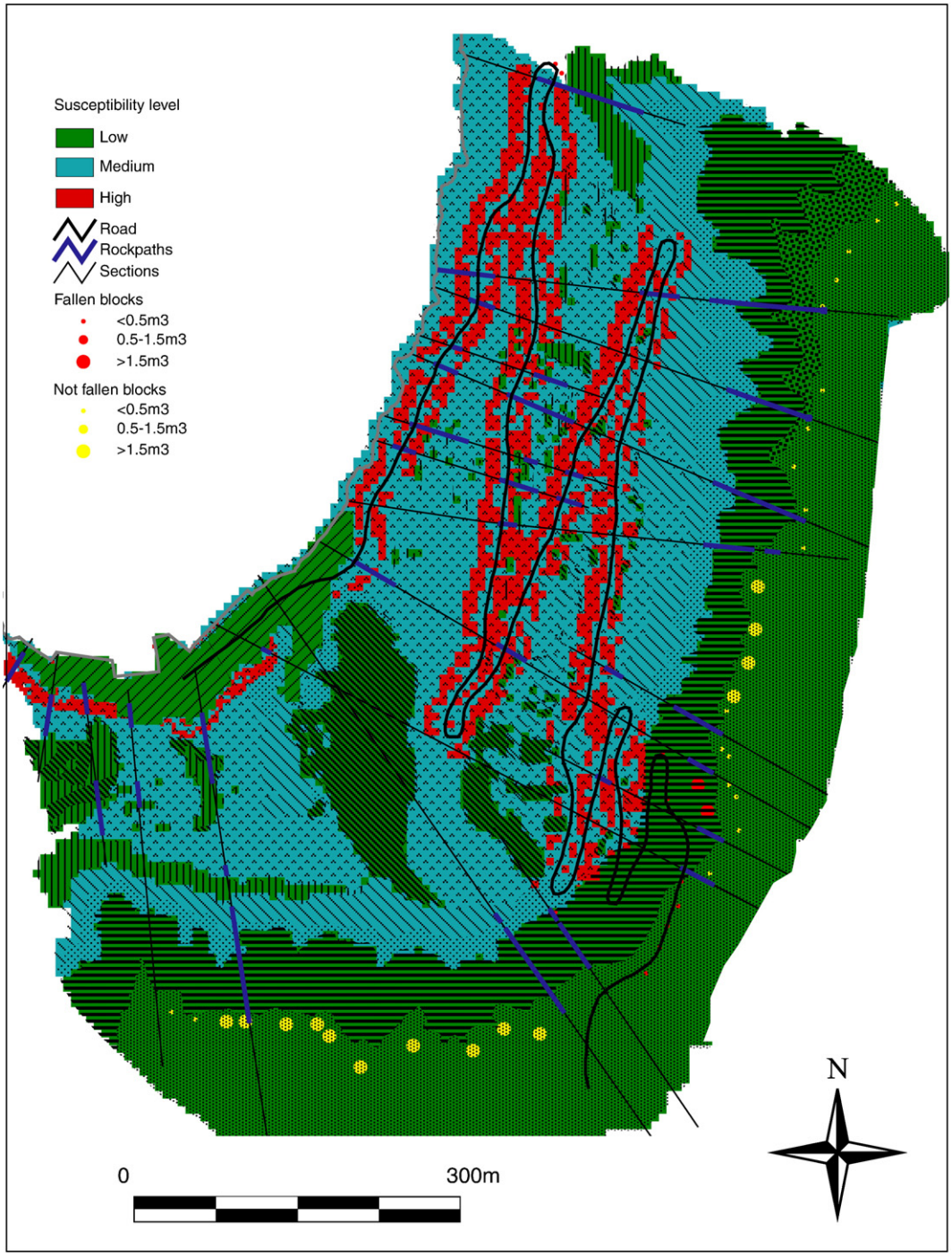

Fig. 14. Rockfall susceptibility map on human activities.

The need for safer use of the road at all elevation levels and in the port facilities denotes the necessity of a 20 m buffer zone along them, thus three zones are entitled to the final rockfall susceptibility map: high, moderate and low susceptibility. Each zone necessitates different protection measures that will be specified in a detailed scale study.

Acknowledgments

The authors would like to sincerely thank the two anonymous reviewers as well as the editor for their help in improving the quality of the manuscript.

References

Agliardi, F., Crosta, G.B., 2003. High resolution three-dimensional numerical modelling of rockfalls. Int. J. Rock. Mech. Min. Sci. 40 (4), 455–471.
Ayala-Cardeco, F.J., Cubillo-Nielsen, S., Alvarez, A., Dominguez, M.J., Lain, L., Lain, R., Ortiz, G., 2003. Large scale rockfall reach susceptibility maps in La Cabrera Sierra (Madrid) performed with GIS and Dynamic Analysis at 1:5, 000. Nat. Haz. 30, 325–340.
Azzoni, A., La Barbera, G., Zaninetti, A., 1995. Analysis and prediction of rockfalls using a mathematical model. Int. J. Rock. Mech. Min. Sci. Geomech. Abstr. 32, 709–724.
Baillifard, F., Jaboyedoff, M., Sartori, M., 2003. Rockfall hazard mapping along a mountainous road in Switzerland using a GIS-based parameter rating approach. Nat. Haz. Earth. Syst. Sci. 3, 431–438.
Broili, L., 1973. In situ tests for the study of rockfall. Geol. Appl. Idrogeol. 8 (1), 105–111 in Italian.

Budetta, P., Santo, A., 1994. Morphostructural evolution and related kinematics of rockfalls in Campania (Southern Italy): a case study. Eng. Geol. 36, 197–210.
Cancelli, A., Crosta, G., 1994. Hazard and risk assessment in rockfall prone areas. In: Skipp, B.O. (Ed.), Risk and Reliability in Ground Engineering. Thomas Telford, pp. 177–190.
Chau, K.T., Wong, R.H.C., Wy, J.J., 2002. Coefficient of restitution and rotational motions of rockfall impacts. Int. J. Rock. Mech. Min. Sci. 39, 69–77.
Chau, K.T., Tang, Y.F., Wong, R.H.C., 2004. GIS Based Rockfall Hazard Map for Hong Kong: Int. J. Rock. Mech. Min. Sci., 41. paper 3B13-SINOROCK Symp.
Chen, C.H., Ke, C.C., Wang, C.L., 2009. A back propagation network for the assessment of susceptibility to rock slope failure in the eastern portion of the Southern Cross-Island Highway in Taiwan. Environ. Geol. 57, 723–733.
Coe, J.A., Harp, E.L., 2007. Influence of tectonic folding on rockfall susceptibility, American Fork Canyon, Utah, USA. Nat. Haz. Earth Syst. Sci. 7, 1–14.
Cook, R., Doornkamp, J., 1990. Geomorphology in environment management: a new introduction. Oxford University Press, Oxford.
Copons, R., Vilaplana, J.M., 2008. Rockfall susceptibility zoning at a large scale: from geomorphological inventory to preliminary land use planning. Eng. Geol. 102, 142–151.
Corominas, J., 1996. The angle of reach as a mobility index for small and large landslides. Can. Geotech. J. 33, 260–271.
Dorren, L.K.A., Seijmonsbergen, A.C., 2003. Comparison of three GIS-based models for predicting rockfall runout zones at a regional scale. Geomorphology 56, 49–64.
Druitt, T.H., Francaviglia, V., 1992. Caldera formation on Santorini and the physiography of the islands in the late Bronze Age. Bull. Volcanol. 54, 484–493.
Environmental Systems Research Institute, (ESRI), 1996. ArcView Spatial Analyst. Advanced Spatial Analysis using Raster and Vector Data. Env Sys Research Ins, USA. 148 pp.
Evans, S.G., Hungr, O., 1993. The assessment of rockfall hazard at the base of talus slopes. Can. Geotech. J. 30, 620–636.
Georgalas, G., 1953. L' eruption du volcan de Santorin en 1950. Bull. Volcanol. 12–13, 39–55.
Giani, G.P., 1992. Rock Slope Stability Analysis. A.A. Balkema, Rotterdam, The Netherlands.
Georgalas, G., Liatsikas, N., 1932. Contribution to the study of the 1925–1926 and 1928 eruptions of Santorini volcano. Bull. Com. Thallassographique of Greece, pp. 1–12.
Georgalas, G., Papastamtiou, J., 1953. L' eruption du volcan de Santirin en 1939–1941. L' eruption du dome Fouque. Bull. Volcanol. 13, 3–38.
Guzzetti, F., Crosta, G., Detti, R., Agliardi, F., 2002. STONE: a computer program for the three-dimensional simulation of rockfalls. Comp. Geosci. 28, 1079–1093.
Hoek E., 2007. Practical rock engineering. Available downloading at http://www.rocsicience.com.
Hoek, E., Bray, J., 1981. Rock Slope Engineering. E & FN Spon, London. Revised 3rd.
Imre, B., Räbsamen, S., Springman, S.M., 2008. A coefficient of restitution of rock materials. Comp. Geosci. 34, 339–350.
ISRM, 1978. Suggested methods for quantitative description of discontinuities in rock masses. International Society for Rock Mechanics, Commission on Standardization of Laboratory and Field Tests. Int. J. Rock. Mech. Min. Sci. Geomech. Abstr. 15, 319–368.
Kobayashi, Y., Harp, E.L., Kagawa, T., 1990. Simulation of rockfalls triggered by earthquakes. Rock. Mech. Rock. Eng. 23, 1–20.
Ktenas, K., 1926a. L' eruption du volcan des Kamenis (Santorin) en 1925. Bull. Volcanol. I (3), 3–64.
Ktenas, K., 1926b. Characteristics of the explosions of Kameni Volcano. Pract. Acad. Athens I, 75–83.
Lan, H., Derek Martin, C., Lim, C.H., 2007. RockFall analyst: a GIS extension for three-dimensional and spatially distributed rockfall hazard modeling. Comp. Geosci. 33, 262–279.
Lin, C.W., Liu, S.H., Lee, S.Y., Liu, C.C., 2006a. Impacts on the Chi-Chi earthquake on subsequent rain-induced landslides in central Taiwan. Eng. Geol. 86 (2–3), 87–101.
Lin, J.C., Petley, D., Jen, C.H., Koh, A., Hsu, M.L., 2006b. Slope movements in a dynamic environment—a case study of Tachia River, Central Taiwan. Quat. Int 147, 103–112.
Lipman, P.W., 1976. Caldera-collapse breccias in the western San Juan Mountains, Colorado. Geol. Soc. Am. Bull. 87, 1397–1410.
Papazachos, B.C., Papazachou, K., 1997. The Earthquakes of Greece. Ziti editions. Thessaloniki, Greece.
Roth, R.A., 1983. Factors affecting landslide susceptibility in San Mateo County, California. Bull. Assoc. Eng. Geol. 20 (4), 353–372.
Rouiller, J.D., Jaboyedoff, M., Marro, C.H., Philippossian, F., Mamin, M., 1998. Pentes instable dans le Pennique valaisan. Rapport final du Programme National de Recherche PNR 31/CREALP, vol. 98. vdf Hochschulverlag AG and ETH, Zürich, Switzerland. in French.
Tataris, A., 1964. The Eocene in the semi metamorphosed basement of Thera Island. Bull. Geol. Soc. Greece VI, 232–237.
Varnes, D.J., 1978. Slope movements: types and processes. In: Schuster, R.L., Krizek, R.J. (Eds.), Landslide Analysis and Control. Transportation Research Board, Special Report No. 176, Washington, DC, pp. 11–33.
Washington, H., 1926. Santorini eruption of 1925. Bull. Geol. Soc. Am. 37, 349–384.